Liquid Crystals
Publication details, including instructions for authors and subscription information:
http://www.informaworld.com/smpp/title~content=t713926090

Dielectric, optical and TSM measurements on semi-perfluoro ferro- and antiferro-electric liquid crystals

S. Sarmento; P. Simeao; Carvalho M. Glogarova; M. R. Chaves; H. T. Nguyen; M. J. Ribeiro

Online publication date: 06 August 2010

To cite this Article Sarmento, S. , Simeao, P. , Glogarova, Carvalho M. , Chaves, M. R. , Nguyen, H. T. and Ribeiro, M. J.(1998) 'Dielectric, optical and TSM measurements on semi-perfluoro ferro- and antiferro-electric liquid crystals', Liquid Crystals, 25: 3, 375 — 385
To link to this Article: DOI: 10.1080/026782998206182
URL: http://dx.doi.org/10.1080/026782998206182

LIQUID CRYSTALS, 1998, VOL. 25, NO. 3, 375–385

Dielectric, optical and TSM measurements on semi-perfluoro ferro- and antiferro-electric liquid crystals

by S. SARMENTO, P. SIMEÃO CARVALHO, M. GLOGAROVÁ†, M. R. CHAVES*, H. T. NGUYEN‡ and M. J. RIBEIRO

Departamento de Física, IMAT (núcleo IFIMUP), CFUP, Faculdade de Ciências da Universidade do Porto, Rua do Campo Alegre 687, 4150 Porto, Portugal

†Institute of Physics, Academy of Sciences of the Czech Republic, Na Slovance 2, 180 40 Prague 8, Czech Republic

‡Centre de Recherche Paul Pascal, A. Schweitzer, 33600 Pessac, France

(*Received 14 February 1998; accepted 9 April 1998*)

Two compounds with very similar chemical formulae but different phase sequences, denoted by **F3H6** and **F4H6**, have been studied by dielectric, optical and TSM measurements, and by optical and polarization hysteresis loops. The light diffraction technique was used to measure the helical pitch (p), which was found to be nearly temperature independent. Six relaxation modes have been identified. The polarization and tilt angle results are discussed using a simple phenomenological model and fitted to the equation

$$\frac{P_0}{\theta_0} \approx \left(\frac{1}{\varepsilon \varepsilon_0 C} - \frac{\Omega}{C} \theta_0^2 \right)^{-1}.$$

The parameters C and Ω were determined from the fitting.

1. Introduction

New liquid crystalline compounds having the general chemical formula:

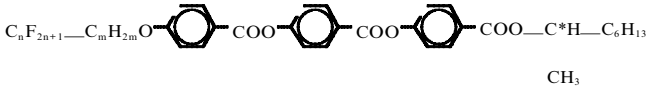

and denoted by **F*n*H*m*** were recently synthesized [1]. These compounds exhibit the ferroelectric SmC* phase and the paraelectric SmA* phase, but the phase transition sequences depend strongly on the length and fluorine composition of the alkoxy chain. This work describes an experimental study on two compounds of this series, namely **F3H6** and the **F4H6**.

A preliminary differential scanning calorimetry (DSC) analysis, as well as optical observations of the textures for homeotropic and planar aligned samples, suggested the following phase sequences:

F3H6: Cr $\xrightarrow{122{\cdot}6^\circ}$ SmC* $\xrightarrow{144{\cdot}6^\circ}$ SmA* $\xrightarrow{151^\circ}$ I

F4H6: Cr $\xrightarrow{108^\circ}$ $\mathrm{SmC_A^*}$ $\xrightarrow{111{\cdot}7^\circ}$ $\mathrm{SmC_{FI}^*}$ $\xrightarrow{112^\circ}$ SmC* $\xrightarrow{150^\circ}$ SmA* $\xrightarrow{158{\cdot}4^\circ}$ I

*Author for correspondence.

The difference between the two phase sequences is a consequence of the so-called odd–even effect [2, 3], which favours the onset of the antiferroelectric or the ferroelectric phases according to the length of the alkoxy chain. The chiral chain of these compounds, on the other hand, always favours the antiferroelectric phase [3].

The temperature scan method (TSM) [4] technique was used to confirm the phase sequences of both compounds. The spontaneous tilt angle, the spontaneous polarization and the helical pitch were obtained as a function of temperature. The relaxation processes were also studied by dielectric and electrooptical measurements.

In the following account we will describe the experimental procedures used in this work. The experimental results for each compound will be discussed separately. The relaxation processes observed for both compounds have been identified.

The simple phenomenological model [5] is used to interpret the polarization and tilt angle temperature dependences. They were determined experimentally using an electric field strong enough to unwind the helix. This enabled us to simplify considerably the expression of the generalized Landau expansion presented in [5]. Accepting that $P_0^3 \ll P_0$, since the highest polarization is about $10^{-3}\,\mathrm{C\,m^{-2}}$ for these compounds, the relation

0267–8292/98 $12·00

between P_0 and θ_0 is [6]:

$$\frac{P_0}{\theta_0} \approx \left(\frac{1}{\varepsilon_0 \varepsilon C} - \frac{\Omega}{C} \theta_0^2 \right)^{-1} \tag{1}$$

where C and Ω are, respectively, the coefficients of the piezoelectric bilinear and biquadratic couplings between the tilt and the polarization, and ε is the relative dielectric constant at high temperature. The experimental results were fitted to equation (1). At the end of this article the results obtained on each compound are compared.

The behaviour of the Goldstone mode dielectric contribution and frequency is now discussed for both compounds. In [5] it has been shown that the equations governing the temperature dependence of the dielectric strength and of the relaxation frequency of the Goldstone mode are:

$$\Delta\varepsilon = \frac{1}{4\pi\varepsilon_0} \frac{p^2}{2\pi K} \left(\frac{P_0}{\theta_0} \right)^2 \tag{2a}$$

$$f = \frac{2\pi K}{p^2 \gamma} \tag{2b}$$

$$\Delta\varepsilon f = \frac{1}{4\pi\varepsilon_0} \frac{1}{\gamma} \left(\frac{P_0}{\theta_0} \right)^2 \tag{2c}$$

where γ is the viscosity associated with the Goldstone mode, ε_0 is the dielectric constant of a vacuum, K is the elastic modulus and p is the helical pitch. From these equations it follows that:

$$\gamma = \frac{1}{4\pi\varepsilon_0} \frac{1}{\Delta\varepsilon\ f} \left(\frac{P_0}{\theta_0} \right)^2 \tag{3a}$$

$$K = \frac{p^2 \gamma f}{2\pi}. \tag{3b}$$

Equations (3*a*) and (3*b*) were used to estimate the temperature dependence of the Goldstone mode viscosity coefficient (γ) and of the elastic modulus (K) in the SmC* phase of both compounds.

2. Experimental

The liquid crystals were filled by capillarity into planar cells (E.H.C. Co, Japan) with a distance between electrodes of 7·5 or 25 μm. The samples were placed in an oven and the temperature was controlled by a Lakeshore DRC-93CA temperature controller or, alternatively, by a programmable power supply (TimeElectronics 9810) linked to a computer. In any case, the accuracy was better than 0·1 K.

The samples were first cooled from the isotropic phase, to some degrees above the transition to the crystalline phase. All the measurements were carried out between this temperature and the SmA*–I transition temperature.

The complex dielectric constant was measured at stabilized temperatures on heating and cooling runs for the frequency range 20 Hz–1 MHz, using an LCR meter (HP4284A). The dielectric data were fitted to the expression [7]:

$$\varepsilon^*(\omega) = \sum_k \frac{\Delta\varepsilon_k}{1 + \left(i \frac{f}{f_k} \right)^{\beta_k}} + \frac{1}{\left(i \frac{f}{f_c} \right)^{\alpha}} \tag{4}$$

where $t_c = 1/f_c$ can be regarded as a characteristic conduction time, by analogy with the characteristic relaxation time $t_k = 1/f_k$. The parameter α indicates the dispersion of the characteristic conduction time ($0 < \alpha < 1$). Such a dispersion results in a capacitance which contributes to the real part of the dielectric constant.

The d.c. conduction observed for the compound **F3H6** is so low that the last term in expression (4) can be ignored. However, for the compound **F4H6** the conductivity at low frequencies has an important effect.

For the TSM measurements we used the set-up described in [4]. When an a.c. electric field is applied to the liquid crystalline sample, the average (d.c.) current flowing in the circuit can be written as [4]:

$$\langle I \rangle = \left\langle \frac{\partial\varepsilon}{\partial T} \frac{\mathrm{d}T}{\mathrm{d}t} \mathbf{E} + \varepsilon \frac{\mathrm{d}\mathbf{E}}{\mathrm{d}t} + \frac{\partial P_s}{\partial t} + \frac{\partial P_s}{\partial T} \frac{\mathrm{d}T}{\mathrm{d}t} + \frac{\partial P_s}{\partial \mathbf{E}} \frac{\mathrm{d}\mathbf{E}}{\mathrm{d}t} + \sigma E_1 \right\rangle S \tag{5}$$

where S is the electrode area. By choosing an adequate a.c. field and changing the temperature at a constant rate it is possible to ensure that the greatest contributions to $\langle I \rangle$ reflect either the polar character of the mesophase or the sudden changes in this polar character which occur at the phase transitions. Therefore this method can reveal the existence of different polar phases in chiral smectics. It is particularly useful for disclosing ferrielectric phases and the alpha phase, which are sometimes difficult to identify by other methods.

Optical and polarization hysteresis loops were obtained for a triangular wave generated by a HP33120A signal generator and amplified by a Kepko (Bop 1000M) signal amplifier. For the optical hysteresis loops, the intensity of the transmitted light was obtained with a BPW21 (R.S. components, Ltd) photodiode.

The electro-optical response was obtained on well aligned samples for the frequency range 1 Hz–100 kHz. The alignment was insured by an electric field treatment at the high temperature limit of the SmC* phase for about half an hour at a frequency of 10–20 Hz.

The helical pitch was measured by the diffraction of laser light (630 nm).

3. Experimental results and discussion

3.1. *The compound* ***F3H6***

3.1.1. *Identification of the phase sequence*

TSM measurements performed on **F3H6** confirmed the phase sequence suggested by DSC. Figure 1 shows the mean value of the electrical current, $\langle I \rangle$, as a function of the temperature. The highest values of $\langle I \rangle$ correspond to the temperature range of the SmC* phase [4], and the transition to the SmA* phase is clearly seen. Measurements on heating and cooling runs revealed no significant thermal hysteresis at this phase transition. This is in agreement with the second order character of the SmC*–SmA* phase transition.

3.1.2. *Polarization and tilt angle*

The spontaneous polarization (P_0) and the tilt angle (θ_0) were calculated from optical and polarization hysteresis loops, respectively. These loops also confirmed the existence of the ferroelectric SmC* phase [8] in **F3H6**.

The temperature dependences of P_0 and θ_0 are presented in figure 2. The inset of figure 2 shows a fit of the experimental data (P_0/θ_0) to equation (1). There is a good agreement between the experimental results and those predicted by the model. The parameters C and Ω were obtained from this fit, while ε was taken from the dielectric measurements. Their values are presented in the table below.

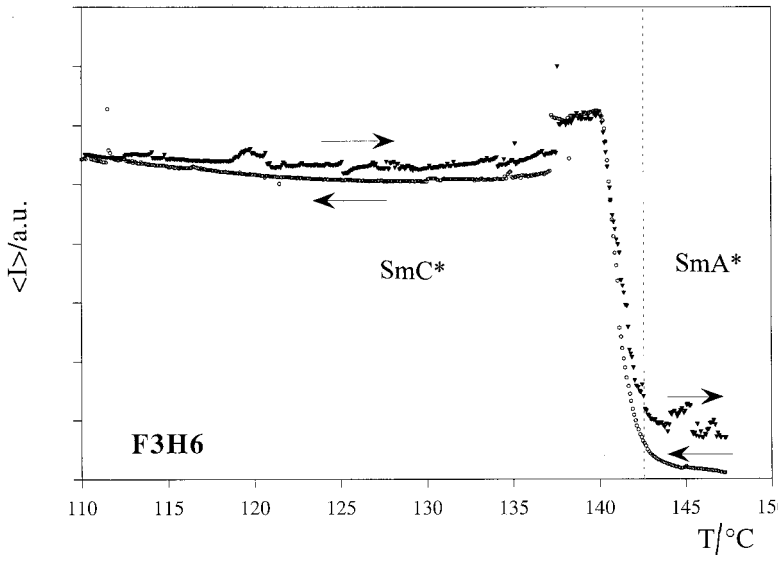

Figure 1. Results of TSM measurements on a 25 μm thick sample of **F3H6**, for heating and cooling runs. The higher values of $\langle I \rangle$ correspond to the temperature range of the ferroelectric SmC* phase. The transition to the SmA* phase is clearly seen and presents no significant thermal hysteresis.

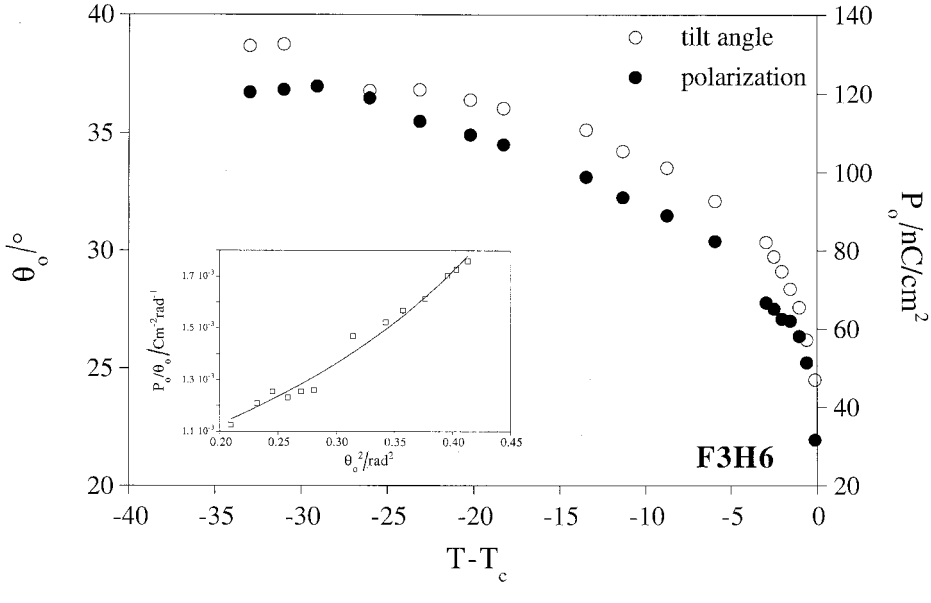

Figure 2. Spontaneous polarization (P_0) and spontaneous tilt angle (θ_0) measured on heating for a 25 μm thick sample of **F3H6**. T_c is the temperature of the SmA*–SmC* phase transition, corresponding to the dashed line of figure 1. The experimental error in the determination of θ_0 is around 8%, while P_0 was calculated with an accuracy better than 10%. The inset shows a fit of the experimental data to equation (1).

Table. Parameters C and Ω obtained from the fit of equation (1) and ε taken from the dielectric measurements for both studied compounds.

Compound	C/V m^{-1}	Ω/C^{-1} V m	ε
F3H6	$2{\cdot}6 \times 10^{7}$	$3{\cdot}9 \times 10^{10}$	3·7
F4H6	$4{\cdot}9 \times 10^{7}$	$7{\cdot}7 \times 10^{10}$	1·7

3.1.3. *Frequency dispersion of the dielectric constant and of the electro-optical response*

Measurements of the electro-optical response were performed on well aligned samples of thickness 7·5 and 25 μm, revealing two relaxation modes with contributions of comparable magnitude. Figure 3 shows the relaxation frequencies of these two modes as a function of temperature. One of them is characterized by a very low relaxation frequency (≈40 Hz), and so has been designated the LF (low frequency) mode. The other is the Goldstone mode, which exhibits a relaxation frequency of about 4 kHz.

The soft mode was not seen in this electro-optical measurement, but it was detected in the SmA* phase by dielectric measurements, as can be seen in figure 4. It exhibits a very high relaxation frequency (>100 kHz) which increases as the temperature increases.

The relaxation frequency of the Goldstone mode obtained by dielectric measurements agrees with that taken from the electro-optical results (see figures 3 and 4). This mode presents a high dielectric contribution for the whole temperature range of the SmC* phase and an almost monodispersive behaviour ($\beta \approx 0{\cdot}95$).

The LF mode was not detected in the dielectric measurement when it was performed on a well aligned 25 μm sample. However, it was seen in a preliminary dielectric measurement on a non-aligned 25 μm sample. In this case a very strong dielectric contribution was observed at the same relaxation frequency as that detected by electro-optical measurement. It seems that the strong electric field used to improve the sample alignment reduces the contribution of the LF mode. The reason why the LF mode is detected in the electro-optical study is that this technique is not affected by the sample conductivity in the low frequency region.

When studying the family of compounds MHFPDBC, MHFPUBC and MHFPHBC, Uehara *et al.* [9] observed a relaxation mode with a high dielectric contribution and a very low, nearly temperature independent relaxation frequency. The origin of this low frequency mode has been attributed to space charges accumulated at the interface between the liquid crystal and the polyimide coating of the cells, and therefore has no relation to any structural motion [9]. Such a relaxation process due to free charges has been previously reported for solids [10].

In our compound, the LF mode also presents a low and nearly temperature independent relaxation frequency, although higher than that reported for the mode of reference [9]. Its dielectric contribution is high when compared with that of the Goldstone mode, but improving the alignment with a strong electric field causes it to decrease considerably. Therefore we think that the LF mode is associated with space charges (ions) accumulated in the neighbourhood of structural defects. The movement of these charges causes a change in the local electric field and thus influences the vibration of the director. Improving the alignment reduces the density of such defects and therefore the dielectric contribution of the LF mode decreases.

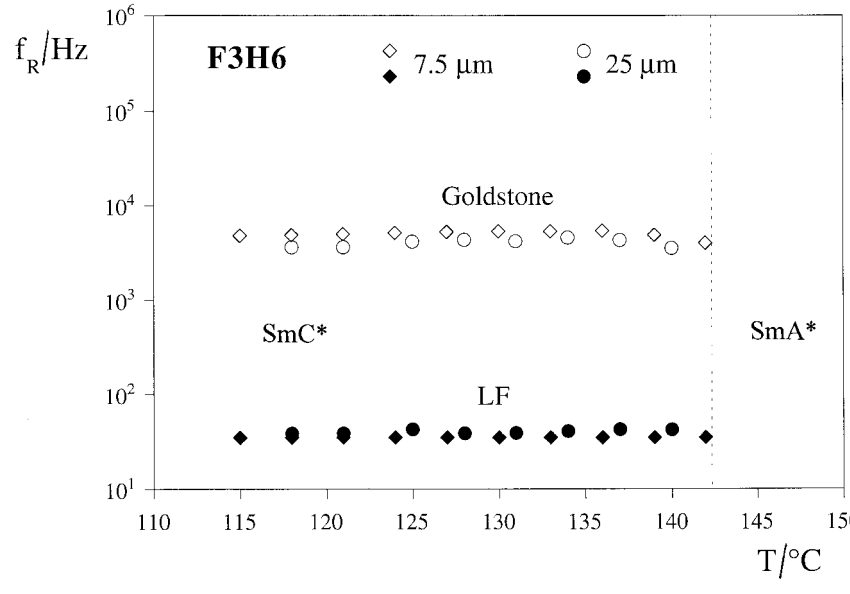

Figure 3. Frequencies of the Goldstone mode (≈4–5 kHz) and LF mode (≈40 Hz) as obtained from electro-optical measurements on the SmC* phase of **F3H6**. The measurement was performed on cooling on well aligned samples of thickness 7·5 μm (diamonds) and 25 μm (circles).

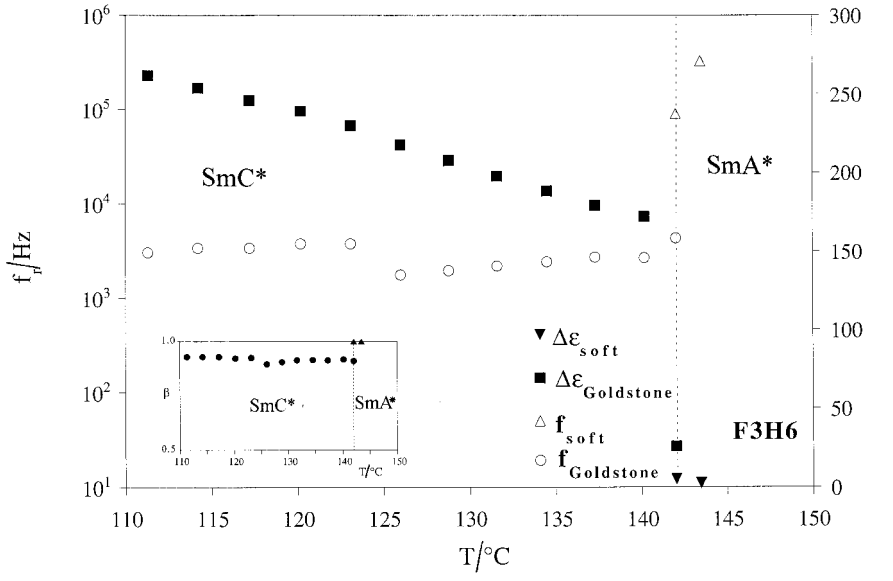

Figure 4. Results of a dielectric dispersion measurement performed on heating, on a 25 μm thick sample of **F3H6**. The LF mode was not detected in this measurement. The Goldstone mode is seen throughout the SmC* phase with a relaxation frequency of ≈2–4 kHz (compare with figure 3, ≈4–5 kHz) and a dispersion parameter $\beta \approx 0{\cdot}95$ (see inset). The soft mode is only seen after the transition to the SmA* phase, and its frequency rises with increasing temperature.

3.2 *The compound* ***F4H6***

3.2.1. *Identification of the phase sequence*

Figure 5 shows the results obtained by TSM on a 25 μm thick sample of **F4H6**. The step indicated by a circle in the high temperature range of figure 5 (between 142 and 147°C) does not coincide with the onset of the SmC* phase. This result can be explained by assuming the occurrence of the SmC^*_α phase in this temperature interval, although it was not detected by DSC.

The small step between the antiferroelectric SmC^*_A and the ferroelectric SmC* phases occurs through a temperature interval of 3 K, considerably larger than the temperature stability range of the ferrielectric SmC^*_{FI} phase (0·3 K) obtained by DSC. Observation of a planar sample by polarizing microscopy without an applied field between 108 and 111°C showed a texture with stripes, which clearly indicates a coexistence of phases near the surfaces. During the TSM measurement this coexistence was not observed, but the applied electric field (0·2 V μm^{-1}, 1 kHz) was probably sufficient to induce some ferroelectric layers near the surfaces, even in the antiferroelectric phase. This explains why the texture observed during the TSM measurement looked quite homogeneous. In this temperature interval we must always consider a phase coexistence of some sort, which probably includes the narrow ferrielectric phase.

TSM measurements on heating and cooling runs showed a thermal hysteresis for the SmC^*_A–SmC^*_{FI} and SmC^*_{FI}–SmC* transitions, suggesting that these are strongly first order (see figure 5).

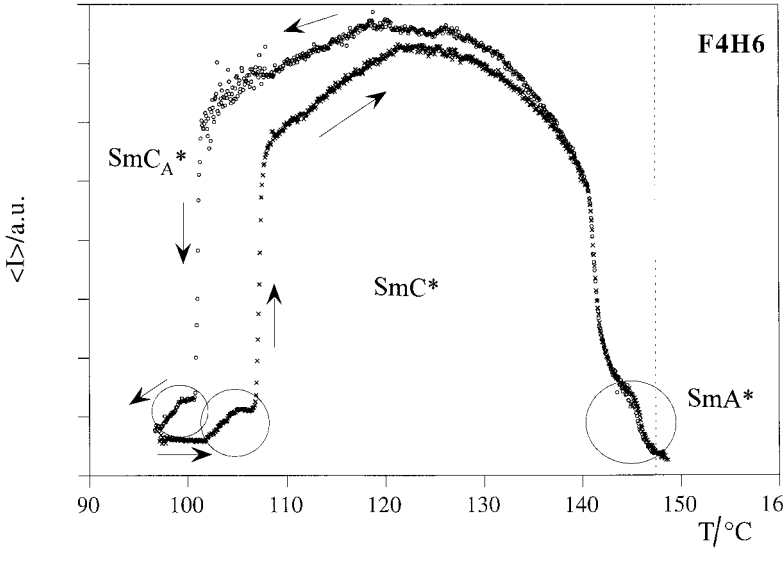

Figure 5. Results of TSM measurements on a 25 μm thick sample of **F4H6**, for heating and cooling runs. The anomaly indicated by a circle between 142 and 147°C may correspond to an alpha-phase. Between the SmC* and the SmC^*_A phases there is a phase coexistence interval, which includes the narrow ferrielectric phase and explains the small step observed. There is a strong thermal hysteresis for the SmC*–SmC^*_{FI} and SmC^*_{FI}–SmC^*_A phase transitions only.

Figure 6 shows optical hysteresis loops obtained at ≈106°C (SmC_A^* phase), ≈109°C (phase coexistence) and ≈123°C (SmC* phase) for **F4H6**. Although they resemble, respectively, typical antiferro-, ferri- and ferroelectric loops [8], some anomalies were observed which are indicated by circles in figures 6(*a*), 6(*b*) and 6(*c*). These anomalies are related to the existence of disclination lines, which could be easily distinguished by the polarizing microscope.

In the temperature range where the alpha phase may occur, between 142 and 147°C, both the optical and polarization hysteresis loops are of the ferroelectric type.

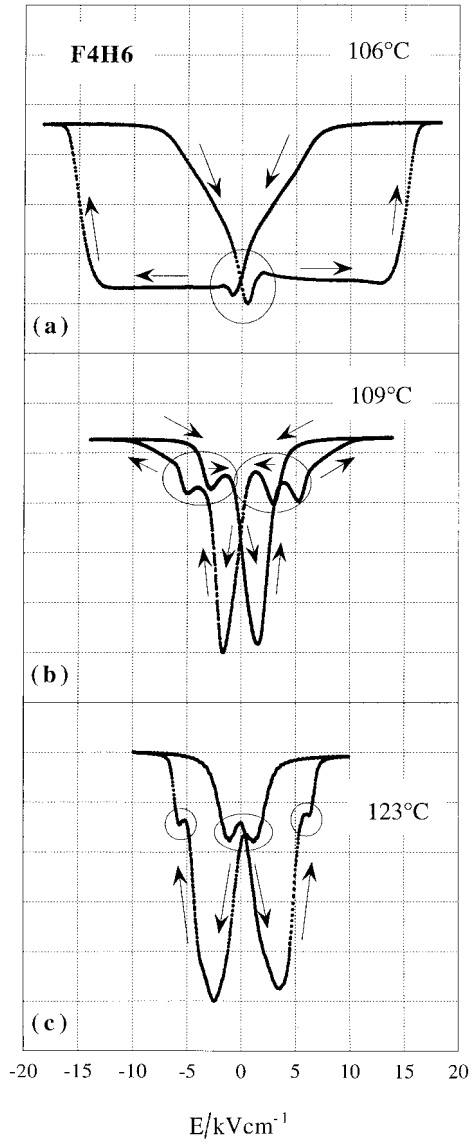

Figure 6. Optical hysteresis loops obtained on a 25 μm thick sample of **F4H6**. The anomalies indicated by circles correspond to the appearance of disclination lines.

3.2.2. *Polarization and tilt angle*

The temperature dependences of the spontaneous polarization (P_0) and the tilt angle (θ_0) are presented in figure 7. The inset shows a fit of the experimental data (P_0/θ_0) to equation (1). There is a good agreement between the experimental results and those predicted by the model, as well as for **F3H6**. The parameters C and Ω were obtained from the fit of the data presented in figure 7, while ε was taken from the dielectric measurements. Their values are presented in the table.

3.2.3. *Frequency dispersion of the dielectric constant and of the electro-optical response*

Electro-optical measurements performed on well aligned 25 and 7·5 μm thick samples revealed the presence of the Goldstone mode and of a low frequency mode in the ferroelectric SmC* phase of **F4H6**. These results are presented in figure 8. The low frequency mode has been designated the LF mode as in the case of **F3H6**. A relaxation mode (designated N mode) with a frequency of ≈400 Hz was observed in the phase coexistence temperature interval (108–111°C) by dielectric measurements on heating only (see below). In the frequency dispersion of the electro-optic response below ≈107°C there is some evidence of this mode, but its contribution could not be separated from the contribution of the Goldstone mode.

The LF mode (≈40 Hz) is assumed to have the same origin in both **F4H6** and **F3H6**, because it presents very similar characteristics. It was not observed by dielectric measurements in **F4H6**, because the presence of a strong d.c. conductivity makes the analysis of the dielectric dispersion data at low frequencies very difficult. The data were fitted to expression (4) and the results of this analysis for a well aligned sample are presented in figures 9 (heating) and 10 (cooling). The dashed lines indicate the temperature interval where a striped texture (phase coexistence) was observed by polarizing microscopy. The transition to the SmA* phase is marked by full lines.

The high frequency (⩾100 kHz) soft mode is seen in the SmA* phase, but its frequency rises quickly beyond the limit of our measurement. This had also happened for **F3H6**.

The Goldstone mode is seen by dielectric measurements throughout the whole temperature range of the SmC* phase (see figures 9 and 10). The relaxation frequency agrees well with the results of the electro-optical measurements, the β parameter varies between $\beta \approx 0{\cdot}85$ and $\beta \approx 0{\cdot}95$ [see figures 9(*c*) and 10(*c*)] and the dielectric contribution is nearly temperature independent [see figures 9(*b*) and 10(*b*)].

The Goldstone mode is also detected in the temperature range of coexistence of the ferro- and antiferro-phases

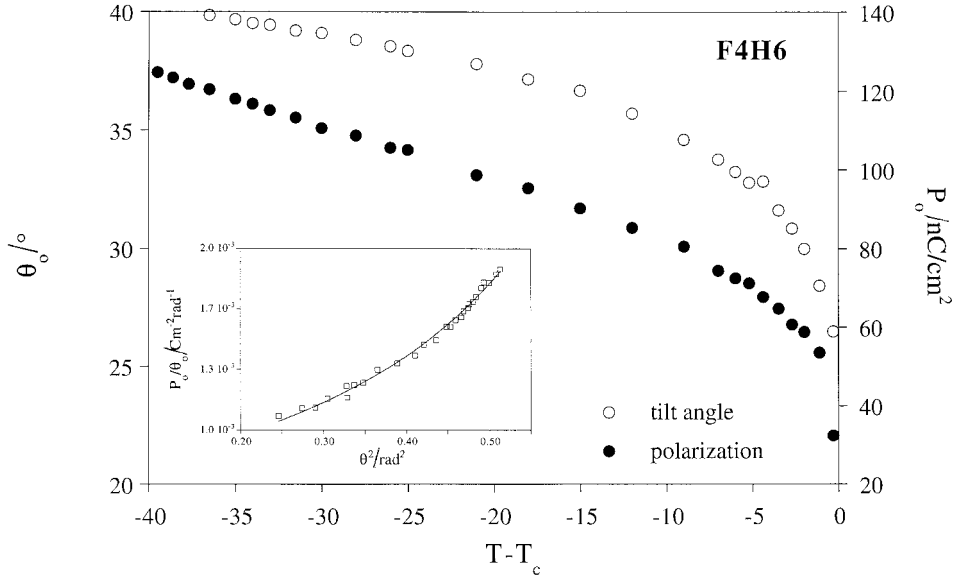

Figure 7. Spontaneous polarization (P_0) and spontaneous tilt angle (θ_0) measured on heating for a 25 μm thick sample of **F4H6**. T_c is the temperature of the transition to the SmA* phase, and corresponds to the dashed line of figure 5. The experimental error in the determination of θ_0 is around 8%, while P_0 was calculated with an accuracy better than 10%. The inset shows a fit of the experimental data to equation (1).

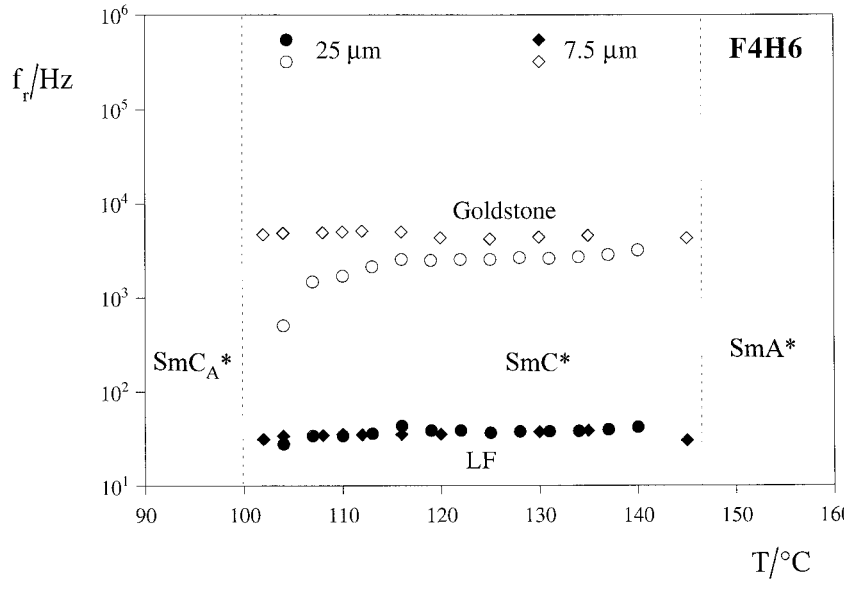

Figure 8. Frequencies of the Goldstone mode (≈2·5 kHz, 25 μm; ≈5 kHz, 7·5 μm) and LF mode (≈40 Hz), as obtained from electro-optical measurements on the SmC* phase of **F4H6**. The measurement was performed on cooling well aligned samples of thickness 7·5 μm (diamonds) and 25 μm (circles). The dashed lines indicate the phase transition temperatures as obtained for a 25 μm sample.

(this range includes the narrow ferrielectric phase), and in this temperature interval it exhibits a considerably lower $\Delta\varepsilon$.

For **F4H6** the relaxation frequency of the Goldstone mode (unlike that of the LF mode) is slightly thickness dependent (see figure 8). Such a behaviour concerning this mode can only be understood if we consider the twist–bend modulation of the director in the smectic layers along the sample plane normal. This modulation, which is imposed by polar surface anchoring, influences the fluctuations of the helix (Goldstone mode) and makes it thickness dependent in such a way that the relaxation frequency increases and the strength of the mode decreases when the sample thickness decreases [11]. This is exactly what has been found experimentally for **F4H6**.

In the phase coexistence temperature interval the N (new) mode presents a relaxation frequency of ≈100–400 Hz and becomes soft near the transition to the SmC* phase. This softening is clearly seen in figures 9(*a*) and 9(*b*). The reason why the N mode was not detected on cooling (figure 10) is not clear.

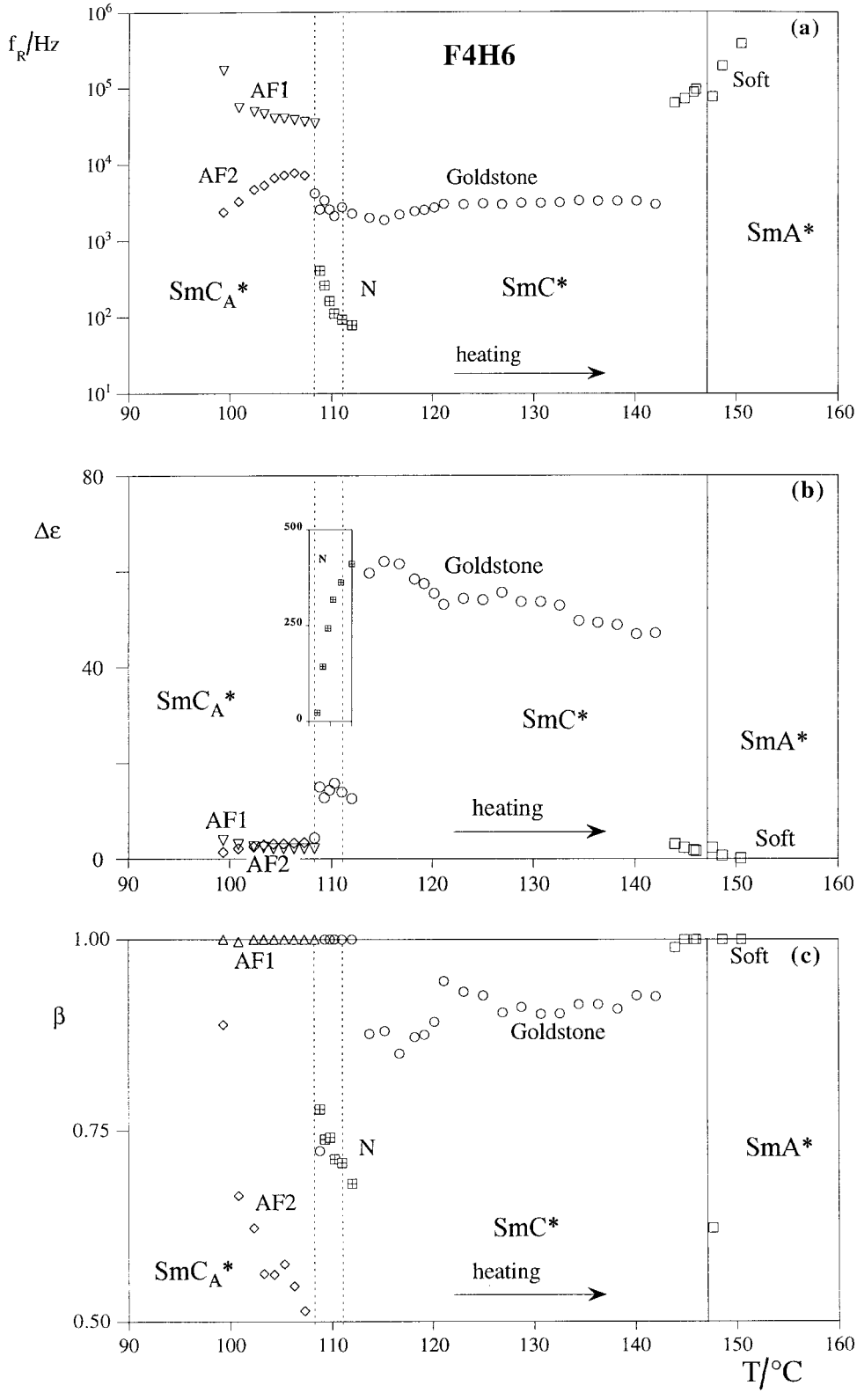

Figure 9. Relaxation frequencies (*a*), dielectric contributions (*b*), and dispersion parameters (*c*) of the relaxation modes found for a 25 μm thick sample of **F4H6**, *on heating*. The dashed lines indicate the temperature intervals where phase coexistence was observed. The temperature of the transition to the SmA* phase is marked with a black line. The dielectric contribution of the N mode is shown in the inset.

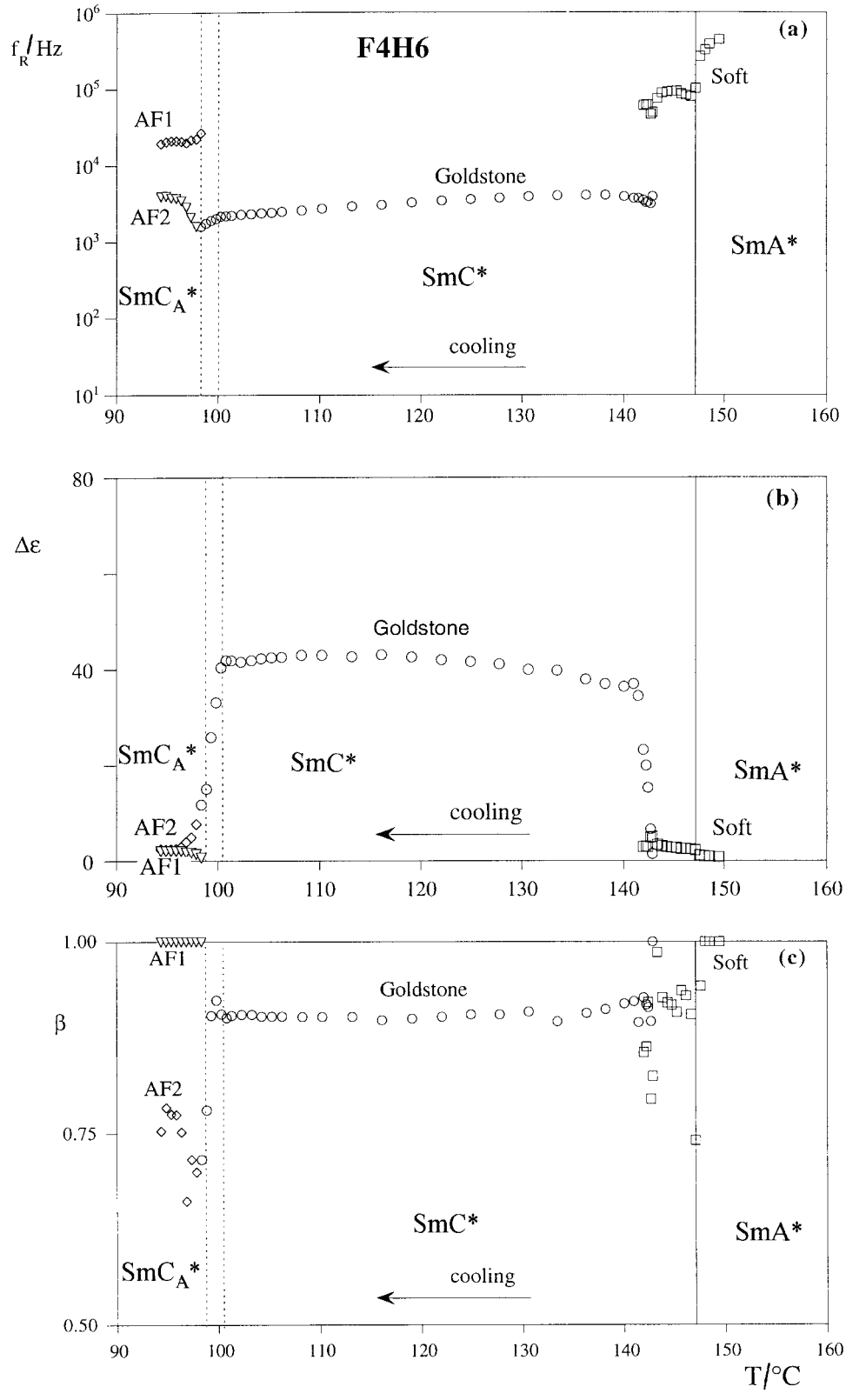

Figure 10. Relaxation frequencies (*a*), dielectric contributions (*b*), and dispersion parameters (*c*) of the relaxation modes found for a 25 μm thick sample of **F4H6**, *on cooling*. The dashed lines indicate the temperature intervals where phase coexistence was observed. The temperature of the transition to the SmA* phase is marked with a black line.

The phase coexistence observed by polarizing microscopy was in the form of a striped texture. This indicates the presence of large (macroscopic) areas of the SmC_A^* phase coexisting with the SmC* phase. The N mode probably corresponds to fluctuations of the boundaries which separate these phases. Its low frequency and large dielectric contribution reflect the size and the number of the regions involved. This is a polydispersive mode due to the non-uniformity of the regions. The ferroelectric regions grow until the transition to the SmC* phase is completed, and hence the mode softens. Modes with a similar behaviour have already been observed in the neighbourhood of ferrielectric phases [8].

Two modes with weak contributions were detected by dielectric measurements in the antiferroelectric phase (see figures 9 and 10). They were designated AF1 and AF2. The first is a true monodispersive mode ($\beta = 1$) with a high relaxation frequency (≈30–100 kHz). AF2 (≈2–8 kHz) is polydispersive and its β parameter shows a pronounced decrease near the phase transition, as shown in figures 9(*c*) and 10(*c*). The nature of these modes will be discussed elsewhere.

In the TSM measurement presented in figure 5, there was an anomaly below the SmA* phase of **F4H6**, between 142 and 147°C. In figure 11 an anomaly can also be seen below the SmA* phase, in the real part of the dielectric constant measured on heating and on cooling for a 25 μm thick sample. In this temperature interval (142–147°C), the Goldstone mode is detected neither by dielectric nor by electro-optical measurements (see figures 8, 9 and 10), but a high frequency mode appears. It was not distinguished from the SmA* phase soft mode in figures 9 and 10, but at the transition to the SmA* phase there is a small jump in the relaxation frequency. A similar discontinuity has been detected at the SmC_α^*–SmA* phase transition of another compound [12], where the SmA* phase soft mode and the so-called 'triggered' mode of the SmC_α^* phase have very different frequencies.

This suggests the existence of the SmC_α^* phase in this temperature range, although this phase was not detected by DSC.

4. Comparison of the two compounds and conclusion

Despite their very similar chemical formulae, the two compounds studied have very different phase sequences. The compound **F4H6** presents a rather wide antiferroelectric phase which is not present in the phase sequence of compound **F3H6**. The experimental measurements of the helical pitch in the SmC* phase as a function of temperature yielded nearly constant and very similar values for both compounds:

$$p = 1{\cdot}00 \pm 0{\cdot}01\ \mu\text{m} \quad \text{for } \mathbf{F3H6}$$

$$p = 0{\cdot}80 \pm 0{\cdot}02\ \mu\text{m} \quad \text{for } \mathbf{F4H6}.$$

The pitch was measured for **F4H6** in the SmC* phase only, because in the temperature range where the SmC_α^* phase may exist (between 142 and 147°C), no conclusive result was obtained.

For a given temperature ($T - T_c$) in the SmC* phase, the values of the spontaneous polarization (P_0) and of the tilt angle (θ_0) are of the same order for the two compounds (see figures 2 and 7). These experimental values were well fitted by equation (1) for both compounds (see insets of figures 2 and 7). The results show

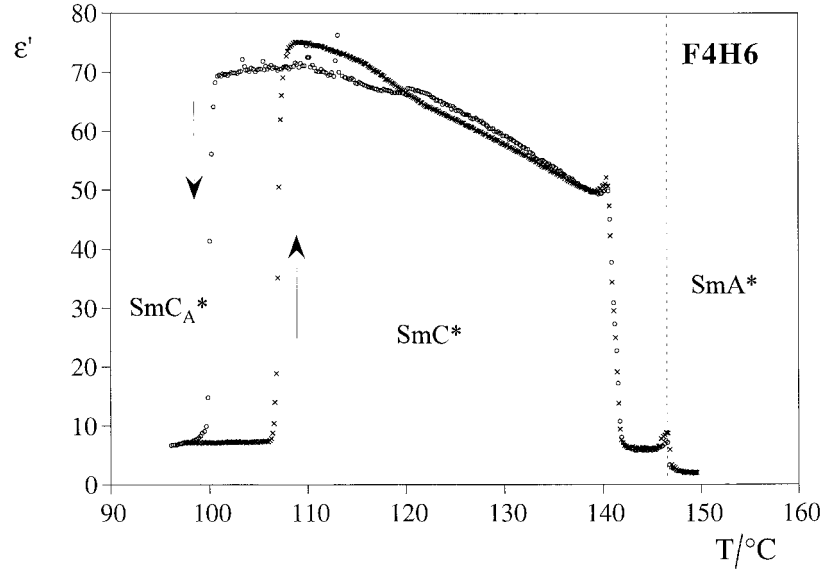

Figure 11. Real part of the dielectric constant, measured at 80 Hz, 1 K min^{-1}, on heating and cooling, for a 25 μm thick sample of **F4H6**.

that P_0/θ_0 is far from being constant, confirming that the biquadratic coupling (the term in Ω) between P_0 and θ_0 is important for describing the temperature behaviour of these quantities for the compounds studied. C and Ω are of the same magnitude for both compounds.

This similarity of behaviour is not surprising, for in spite of their different phase sequences, the two compounds have very similar chemical formulae. The relaxation processes detected in the ferroelectric SmC* and in the paraelectric SmA* phases are also analogous for both compounds.

The soft mode is seen for both compounds in the paraelectric SmA* phase. Its frequency rises quickly above 1 MHz.

In the ferroelectric phase, the Goldstone mode exhibits a lower frequency and a lower dielectric contribution for **F4H6** than for **F3H6** (see figures 4 and 10). This is a result of different values of the Goldstone mode viscosity coefficient (γ) and of the elastic modulus (K). These quantities were estimated using equations (3). At $\approx$6°C below the transition to the SmA* phase, $K(\mathbf{F3H6}) \approx 1{\cdot}6 \times 10^{-11}$ N and $K(\mathbf{F4H6}) \approx 3 \times 10^{-11}$ N, while $\gamma(\mathbf{F3H6}) \approx 0{\cdot}04$ Pa s and $\gamma(\mathbf{F4H6}) \approx 0{\cdot}1$ Pa s (*cf.* $\gamma = 0{\cdot}25$ Pa s in reference [6]).

Another mode was detected in the SmC* phase, namely the LF mode, which exhibits a similar behaviour for both compounds.

In the antiferroelectric SmC_A^* phase of **F4H6**, two relaxation processes were detected (designated AF1 and AF2). Their nature will be discussed elsewhere.

The N mode detected on heating between 108 and 111°C in **F4H6** seems to be related to the coexistence of phases near the surface in that temperature interval.

TSM and dielectric measurements showed the existence of an anomaly occurring just below the SmA* phase of **F4H6**. This may indicate the presence of the SmC_α^* phase which was not detected by DSC.

The authors are grateful to Albano Costa for technical assistence. This work was supported by the project PRAXIS XXI/3/3.1/MMA/1769/95. M. Glogarová thanks the Grant Agency of the Czech Republic for Grant no. 202/96/1687 and S. Sarmento thanks project PRAXIS XXI for Grant BD/9545/96.

References

[1] Nguyen, H. T. *et al.* (to be published).
[2] Fukuda, A., Takanishi, Y., Isozaki, T., Ishikawa, K., and Takezoe, H., 1994, *J. Mater. Chem.*, **4,** 997.
[3] Faye, V., Rouillon, J. C., Destrade, C., and Nguyen, H. T., 1995, *Liq. Cryst.*, **19,** 47.
[4] Carvalho, P. S., Glogarová, M., Chaves, M. R., Destrade, C., and Nguyen, H. T., 1996, *Liq. Cryst.*, **21,** 115.
[5] Levstik, A., Carlsson, T., Filipič, C., Levstik, I., Zeckš, B., 1987, *Phys. Rev. A*, **35,** 3527; Carlsson, T., Zeckš, B., Filipič, C., and Levstik, A., 1990, *Phys. Rev. A*, **42,** 877.
[6] Goodby, J. W., Blinc, R., Clark, N. A., Lagerwall, S. T., Osipov, M. A., Pikin, S. A., Sakurai, T., Yoshino, K., and Zeckš, B., 1991, *Ferroelectric Liquid Crystals—Principles, Properties and Applications*, Vol. 7, *Ferroelectricity and Related Phenomena* (Amsterdam: Gordon and Breach Science Publishers).
[7] Fukui, M., Orihara, H., Suzuki, A., Ishibashi, I., Yamada, Y., Yamamoto, N., Mori, K., Nakamura, K., and Suzuki, Y., 1990, *Jpn. J. appl. Phys.*, **29,** 329.
[8] Carvalho, P. S., Glogarová, M., Chaves, M. R., Nguyen, H. T., Destrade, C., Rouillon, J. C., Sarmento, S., and Ribeiro, M. J., 1996, *Liq. Cryst.*, **21,** 511.
[9] Uehara, H., Hanakai, Y., Hatano, J., Saito, S., and Marashiro, K., 1995, *Jpn. J. appl. Phys.*, **34,** 5424.
[10] Lines, M. E., and Glass, A. M., 1977, *Principles and Applications of Ferroelectrics and Related Materials* (Oxford: Oxford University Press).
[11] Novotná, V., Glogarová, M., Bubnov, A. M., and Sverenyak, H., 1997, *Liq. Cryst.*, **23,** 511.
[12] Destrade, C., Carvalho, P. S., and Nguyen, H. T., 1996, *Ferroelectrics*, **177,** 161.